



PAPER

OPEN ACCESS







RECEIVED
16 October 2024REVISED
2 January 2025ACCEPTED FOR PUBLICATION
30 January 2025PUBLISHED
19 February 2025

Original Content from
this work may be used
under the terms of the
[Creative Commons
Attribution 4.0 licence](#).

Any further distribution
of this work must
maintain attribution to
the author(s) and the title
of the work, journal
citation and DOI.



Demonstration of ultra-high dose rate electron irradiation at FLASHlab@PITZ

X-K Li^{1,*} , Z Amirkhanyan¹, A Grebinyk^{1,2}, M Gross¹, Y Komar^{1,2} , F Riemer¹, A Asoyan^{1,4}, P Boonpornprasert¹, P Borchert² , H Davtyan^{1,4}, D Dmytriiev¹ , M Frohme², A Hoffmann¹, M Krasilnikov¹, G Loisch³ , Z Lotfi^{1,5} , F Müller¹, M Schmitz³, F Obier³, A Oppelt¹, S Philipp¹, C Richard¹, G Vashchenko¹, D Villani¹, S Worm¹ and F Stephan¹

¹ Deutsches Elektronen-Synchrotron DESY, Platanenallee 6, 15738 Zeuthen, Germany

² Technical University of Applied Sciences Wildau, 15745 Wildau, Germany

³ Deutsches Elektronen-Synchrotron DESY, Notkestr. 85, 22607 Hamburg, Germany

⁴ On leave from CANDLER Synchrotron Research Institute, Yerevan, Armenia.

⁵ On leave from Brandenburgische Technische Universität Cottbus-Senftenberg, 03046 Cottbus, Germany.

* Author to whom any correspondence should be addressed.

E-mail: xiangkun.li@desy.de

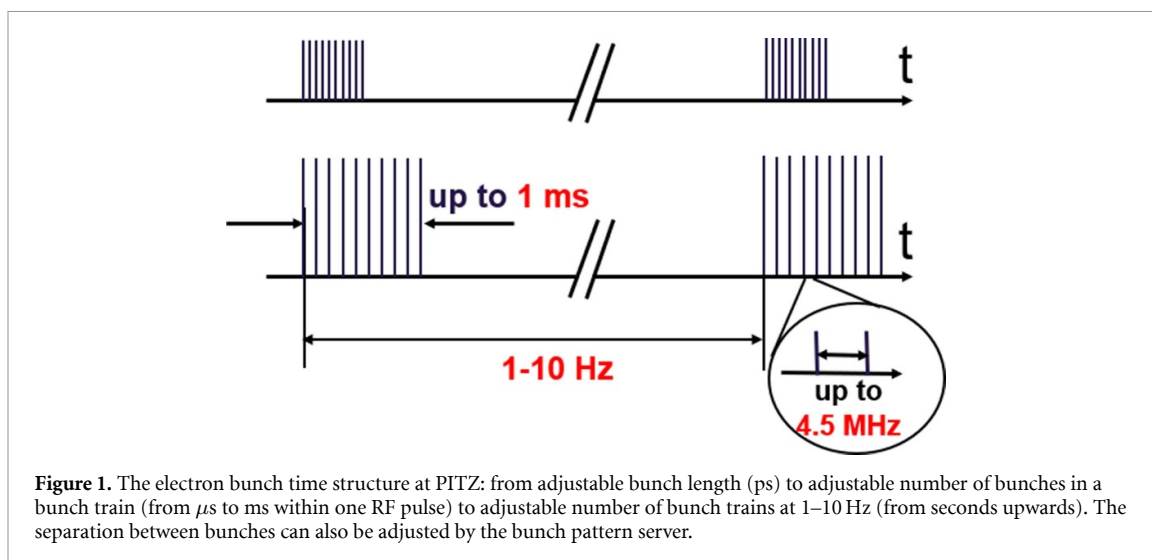
Keywords: ultra-high dose rate, FLASH effect, electron beams, FLASHlab@PITZ

Abstract

Objective. The photo injector test facility at DESY in Zeuthen (PITZ) is building up an R&D platform, known as FLASHlab@PITZ, for systematically studying the FLASH effect in cancer treatment with its high-brightness electron beams, which can provide a uniquely large dose parameter range for radiation experiments. In this paper, we demonstrate the capabilities by experiments with a reduced parameter range on a startup beamline and study the potential performance of the full beamline by simulations. **Approach.** To measure the dose, Gafchromic films are installed both in front of and after the samples; Monte Carlo simulations are conducted to predict the dose distribution during beam preparation and help understand the dose distribution inside the sample. Plasmid DNA is irradiated under various doses at conventional and ultra-high dose rate (UHDR) to study the DNA damage by radiations. Start-to-end simulations are performed to verify the performance of the full beamline. **Main results.** On the startup beamline, reproducible irradiation has been established with optimized electron beams and the delivered dose distributions have been measured with Gafchromic films and compared to FLUKA simulations. The functionality of this setup has been further demonstrated in biochemical experiments at conventional dose rate of 0.05 Gy s^{-1} and UHDR of several 10^5 Gy s^{-1} and a varying dose up to 60 Gy, with the UHDR experiments finished within a single RF pulse (less than 1 millisecond); the observed conformation yields of the irradiated plasmid DNA revealed its dose-dependent radiation damage. The upgrade to the full FLASHlab@PITZ beamline is justified by simulations with homogeneous radiation fields generated by both pencil beam scanning and scattering beams. **Significance.** With the demonstration of UHDR irradiation and the simulated performance of the new beamline, FLASHlab@PITZ will serve as a powerful platform for studying the FLASH effects in cancer treatment.

1. Introduction

Cancer and its treatment are huge challenges, accounting for close to 20 million new cases and 9.7 million deaths globally in 2022 (Bray *et al* 2024). Radiation therapy (RT), meaning irradiation of tumors with high energy particle beams or x-rays, proves highly cost-effective and is an important component of cancer health care, for instance, it accounts for almost 60% of cancer patient treatments in Germany (Beckmann 2020). Normal tissue toxicity remains a major limiting factor for applying RT while cancer metastasizing and radiation resistance challenge its treatment outcome (Schulz *et al* 2019, Kacem *et al* 2022, Kilmister *et al*



2022). Ultra-high dose rate (UHDR) irradiation exhibits normal tissue-sparing ability as compared to the clinically applied conventional dose rate, maintaining at the same time tumor treatment efficiency. This phenomenon, rediscovered in 2014 by Favaudon *et al* (2014), was coined as the ‘FLASH effect’ and was further demonstrated for photon (Montay-Gruel *et al* 2018, Gao *et al* 2022), proton (Patriarca *et al* 2018, Beyreuther *et al* 2019, Diffenderfer *et al* 2020, Zhang *et al* 2020, Cunningham *et al* 2021, Darafsheh *et al* 2021) and electron (Favaudon *et al* 2014, Montay-Gruel *et al* 2017, Schüler *et al* 2017, Bourhis *et al* 2019, Lempart *et al* 2019, Vozenin *et al* 2019) radiation on mice (Favaudon *et al* 2014, Montay-Gruel *et al* 2017), rats (Konradsson *et al* 2022), cats and pigs (Vozenin *et al* 2019, Bley *et al* 2022). Besides its advantageous biological effects, FLASH RT is an attractive approach for clinical translation due to its fast procedure, reduced treatment time and costs. From 2020, the first clinical trials on proton FLASH RT focus on the assessment of its feasibility, toxicity and pain relief for the bone metastasis treatment (Daugherty *et al* 2023, 2024).

At the photo injector test facility at DESY in Zeuthen (PITZ), photoinjector R&D has been conducted for more than 20 years. The resulting excellent electron beam properties are ideally suited to investigate the yet unknown mechanism of the FLASH effect. To this end an R&D platform for electron FLASH cancer RT and radiation biology is being prepared, known as FLASHlab@PITZ (Stephan *et al* 2022).

The PITZ photoinjector consists of an L-band RF gun with a semiconductor photocathode, a cut-disk-structure (CDS) booster accelerator, and various magnets for beam transport and devices for beam diagnostic, e.g. energy spectrum, transverse and longitudinal phase spaces, and time-resolved measurements with better than picosecond resolution. The gun provides a peak gradient up to 60 MV m^{-1} on the cathode surface, accelerating the electron beam to a maximum beam energy of 6.2 MeV, which is then increased to up to 22 MeV by the booster. The electrons are emitted from the semiconductor photocathode (Cs_2Te) driven by a UV laser pulse (photoelectric effect), therefore the electron bunch time structure is defined by that of the laser pulses, as shown in figure 1. With the huge bunch charge range from sub-picocoulomb to a few nanocoulomb and the flexible control of the electron bunch due to its high quality, the PITZ accelerator can provide a uniquely wide parameter space of doses and dose rates, making it a powerful platform for systematically studying the FLASH effects in cancer treatment.

As shown in figure 1, the PITZ photoinjector can provide electron beams or doses for radiation experiments in three different ways, namely, single bunch, multi-bunches in a single train, and single- or multi-bunches in multi-trains. Here, a train refers to one or more electron bunches of picoseconds (ps) length in time, which are separated by 222 nanoseconds (ns) to several microseconds (μs) and are emitted within one RF pulse of up to 1 millisecond (ms) length. A new bunch pattern server also allows to choose almost any arbitrary electron bunches along the train. Combining the properties of a single electron bunch (as given in table 1) and the pulse train time structure, the PITZ accelerator can deliver radiations in a huge span of doses and dose rates, as summarized in table 2 by assuming a beam energy of 20 MeV and an irradiation volume of 1 cm^3 .

Compared to other electron sources for FLASH RT, the PITZ accelerator is highlighted by its large range of bunch charge and the flexible bunch time structure within one RF pulse, which together allow tuning both the dose and dose rate by several orders of magnitude for UHDR radiation (see the multi bunches in single train mode in table 2). For instance, considering 10 Gy in 1 cm^3 volume, the required bunch charge will be at

Table 1. Properties of the electron bunch at PITZ. The full-width at half maximum (FWHM) is given for the duration and the root-mean-square (RMS) is given for the beam size.

Property	Value
Energy	<22 MeV
Charge	0.1 pC to 5 nC
Duration	0.1–45 ps
Beam size	0.02–a few mm

Table 2. Dose parameter space for radiation experiments at PITZ, assuming a beam energy of 20 MeV and an irradiation volume of 1 cm³. The lower limit is estimated with 0.1 pC and the upper limit with 5 nC.

Mode	# of e ⁻ bunches	Duration	Dose, Gy	Dose rate, Gy s ⁻¹
Single bunch	1	0.1–45 ps	10 ⁻⁴ –10	10 ⁷ –10 ¹² ^a
Multi bunches in single train	2–4500	0.22 μs–1 ms	10 ⁻⁴ –10 ⁴	10 ² –10 ⁷ ^b
Multi trains	>1	>0.1 s	>10 ⁻⁴	10 ⁻³ –10 ⁵ ^c

^a Averaged over a single electron bunch.

^b Averaged over a bunch train (RF pulse).

^c Averaged over multiple RF pulses.

least 10 nC (for stopping power ~ 0.2 MeV cm² g⁻¹). This can be realized by a minimum of 2 bunches (5 nC each bunch) to a maximum of 4500 bunches (2.2 pC each bunch) and the corresponding dose rate ranges from 10⁴ to 10⁷ Gy s⁻¹. Commercially available small accelerators such as 6 or 9 MeV Mobertron (Moeckli *et al* 2021) generate electrons from a thermionic cathode operating in a RF pulse of only a few us long. The dose rate in one RF pulse is thus in the order of magnitude of 10⁶–10⁷ Gy s⁻¹. Since the repetition rate of the RF pulses can be up to 1 kHz, it can also deliver 10 Gy with 2–200 RF pulses with a reduced average dose rate between 50 and 10⁴ Gy s⁻¹. Photoinjector-based accelerators are also available for FLASH RT in other facilities, such as the CERN linear electron accelerator for research (CLEAR) and the electron linac for beams with high brilliance and low emittance (ELBE) from Helmholtz-Zentrum Dresden-Rossendorf (HZDR). At CLEAR, the electron bunch (30–220 MeV) repeats at a frequency of 1.5 or 3 GHz with a maximum of 200 bunches and a maximum of 87 nC pulse charge (Korysko *et al* 2023). Like PITZ, the UHDR is provided with one pulse and the corresponding dose rate is in the order of magnitude of 10⁸–10⁹ Gy s⁻¹. At ELBE, the electron bunch (≤ 40 MeV) has a repetition rate of 13 MHz operating in CW mode or in macro pulse mode, with a typical dose rate of 10⁵ Gy s⁻¹ averaged in the macro pulse. Since the separation and length of the macro pulses are adjustable, ELBE can provide a tunable dose rate from 200 Gy s⁻¹ to 10⁵ Gy s⁻¹ for UHDR radiation experiments (Metzkes-Ng *et al* 2023).

Currently, a startup beamline is in operation for radiation experiments at PITZ, where the electron beam is deflected by a dipole magnet to the exit window and the following experimental area. Dosimetry studies and the first *in vitro* experiments have been carried out on this beamline.

Since its performance is limited by the dispersion from the dipole magnet, the startup beamline will be replaced by a full beamline to realize the full dose parameters shown in table 2. The full beamline has been designed to preserve the high beam quality from the PITZ accelerator and will allow reaching more flexible electron beam parameters with better control (Li *et al* 2022). One highlight of the full beamline is that a 2D sweeper will be installed to scan the electron bunches in the transverse plane, enabling the generation of arbitrary dose distributions within a maximum time of 1 ms. Recently, the physics design has been modified for engineering realization, particularly the locations and strengths of dipole and quadrupole magnets, which are the most critical components for achieving the designed beam quality. Start-to-end simulations have been performed to demonstrate the capabilities of this beamline at two distinct bunch charges: (1) low charge (typically 10 pC, space charge effects are weak) for uniform radiation at conventional dose rates and for pencil beam scanning (PBS) at UHDR, and (2) high charge (typically 1 nC, space charge effects are strong) for uniform radiation at UHDR.

2. Materials and methods

2.1. The startup beamline

The startup beamline has been operational at PITZ since 2022, on which dosimetry studies and first irradiation experiments have been performed to demonstrate the capabilities of PITZ electron beams (Li *et al* 2024). As shown in figure 2, the electron beam is bent by a 60 degree dipole magnet and guided through a vertical kicker and diagnostics devices, such as beam position monitors (BPMs), integrated current

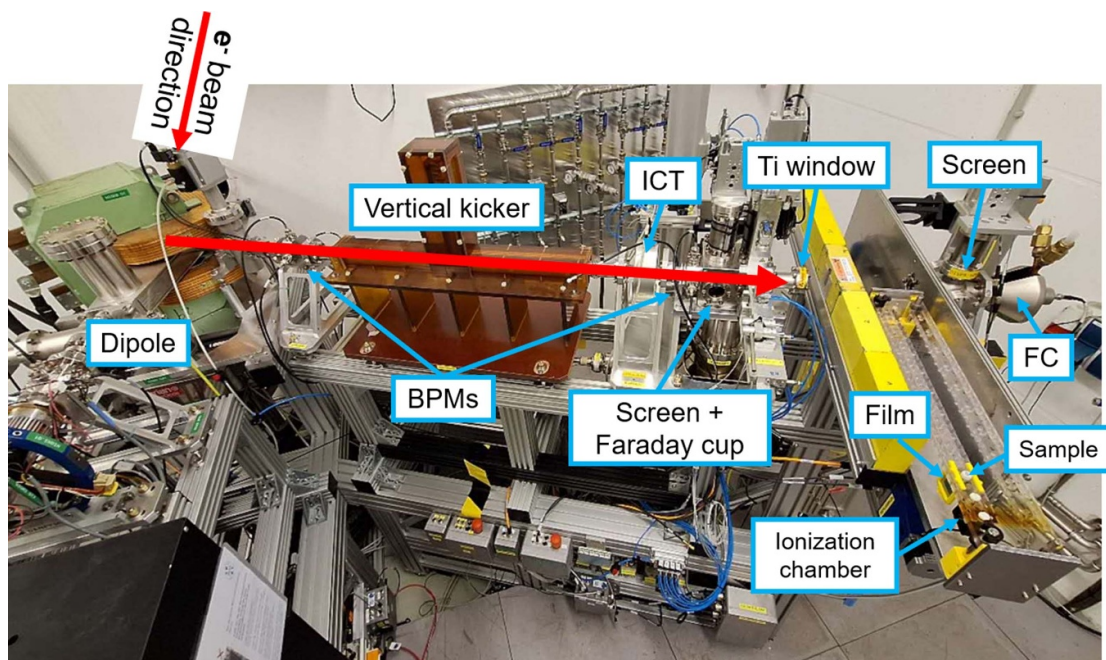


Figure 2. The startup beamline for FLASHlab@PITZ. The electron beam comes from the top, then deflected by a dipole to the right and extracted with a titanium window of $50\ \mu\text{m}$ thickness. Between the dipole and the window, there are diagnostic devices, including two BPMs, one ICT, one screen and one FC. After the window, the beam can be scattered with an insertable scattering plate, collimated by a lead brick with a hole of 30 mm in diameter. There is a second screen station and Faraday cup after the motor stage, where Gafchromic films, samples and an ionization chamber are installed.

transformer (ICT), Faraday cups (FCs), and monitor screen. A Titanium window is used to extract the beam to the experimental area. The kicker is foreseen for scanning electron beams in the vertical direction. Lead bricks are installed after the window to stop the tails of the beam. The samples are usually irradiated in 0.5 ml or 2 ml tubes. A movable sample holder containing up to 10 samples can move the samples one after the other into the beam path for irradiation under different doses & dose rates. The last slot can be occupied by an ionization chamber (IC) for online dose measurement. A second Faraday cup is installed after the samples to measure the bunch charge for dose simulation.

Due to the dispersion from the dipole magnet, the electron beam has a large size (typically around 4 mm RMS) at the exit window, especially for high bunch charge in UHDR radiation experiments. The bunch charge was typically 10 pC and 1 nC for the conventional and UHDRs, respectively. The corresponding beam current within the RF pulse was $10\ \mu\text{A}$ and 1 mA, respectively. Due to the large beam size and the scattering effects from the exit window, a big fraction of the bunch charge is subsequently lost at the lead brick. Despite this, UHDR up to $10^6\ \text{Gy s}^{-1}$ has been achieved in addition to the conventional dose rate of $0.05\ \text{Gy s}^{-1}$.

2.2. Dose measurement with Gafchromic films

To measure the delivered dose for each sample individually, one Gafchromic film is placed in front of each tube as well as one film behind each tube. This allows measuring the entrance and also the exit dose distribution. Regular measurements with small films inside of the tubes are performed to calibrate the dose delivered within the sample with the films in front of and behind the tube.

Gafchromic films are commonly used in UHDR environments because of their dose rate independence. They allow absolute dosimetry and have a spatial resolution down to a few μm . The Gafchromic films used at FLASHlab@PITZ are EBT-XD films from the company Ashland (“[GAFCHROMIC™ DOSIMETRY MEDIA, TYPE EBT-XD, Specification and User Guide](#)”). They have a dynamic range from 0.1 Gy up to 60 (or sometimes 200) Gy and an optimum range of 0.4 Gy up to 40 Gy according to the manufacturer. These films consist of a $25\ \mu\text{m}$ thick active layer of marker dye, stabilizers, and other components sandwiched between $125\ \mu\text{m}$ thick matte polyester substrates.

To do reliable absolute dosimetry, each batch of films needs a new calibration due to differences in composition and thickness of the active layer. Within each batch, the response is consistent. The calibration needs to be done in a homogeneous and well-defined radiation field, that is usually only given in a clinical environment. The calibration of the films used at FLASHlab@PITZ was done at the Charité, a university hospital in Berlin. A clinical, commercially available RT device from the company Varian was used. It can provide a homogeneous radiation field of a size of 25 by 25 cm^2 . The films were placed in this field and

sandwiched between multiple scattering plates (solid water). In addition, reference dosimetry was done using an IC (Semiflex Chamber, Type 31013) from PTW in combination with a PTW Unidos electrometer. The calibration is traceable to the German National Metrology Institute (PTB). The dose rate used was 0.1 Gy s^{-1} , the maximum dose rate this device can provide, for a homogeneous field of 25 by 25 cm^2 .

Multiple films were irradiated with doses between 0.1 Gy and 300 Gy, and all data points were fitted according to equation (1) and aligned well with the fitted curve, although the recommended maximum dose from the manufacturer was up to 200 Gy. There is a known time-dependent darkening effect of the films. The common and recommended procedure is to do the readout 24 h after irradiation. The manufacturer recommends a 48-bit color depth flatbed color scanner for the digitalization of Gafchromic films. At PITZ a professional flatbed scanner, the Epson Expression 12000XL is used for the scanning of the irradiated films. The scanner comes with a transparency unit that makes it suitable to scan films with a color depth of 16 bits per channel (red, green, blue). Large scanners are recommended to decrease lateral effects. Additionally, only the central area is used for film scanning. Scanning the calibration films gives the calibration curve that is unique for the combination of scanner and film batch. The calibration curve is then fitted to a function of the form (GAFCHROMIC™ DOSIMETRY MEDIA, TYPE EBT-XD, Specification and User Guide),

$$P_x(D) = a + \frac{b}{D-c}, \quad (1)$$

where $P_x(D)$ is the scanner response in scanner channel x at dose D ; a , b and c are parameters to be fitted. The inverse of the response function is then used to calculate the dose on the film.

2.3. Monte Carlo simulation using the FLUKA code

The Gafchromic films cannot return the dose immediately because of the waiting time of 24 h, therefore predicting the correct dose and dose distribution during radiation experiments is very important. To achieve this, Monte Carlo simulations using the FLUKA code (Fasso *et al* 2005) have been established by recreating the experimental setup in the simulation, which includes the exit window, the lead brick, the insertable scattering plate, the sample holder, tubes and Gafchromic films. The simulated dose distributions can be compared to measurements by Gafchromic films in front of and behind the tubes.

To make our simulations more accurate, the beam profile measured from a Yttrium aluminum garnet (YAG) screen placed 143 mm before the exit window is used as the initial beam profile. The horizontal divergence is dominated by dispersion and the vertical divergence by betatron motion. The distance from the exit window to the tube is 145 mm. It is crucial to have a uniform dose distribution when irradiating samples. Therefore, FLUKA simulations were performed also to determine the optimal beam profile at the YAG screen to ensure uniform dose distribution in the sample.

2.4. In vitro experiments on plasmid DNA

2.4.1. Reagents and equipment

The plasmid DNA pBR322 (4361 bp) and DNA marker (1 kb) were obtained from Thermo Fisher Scientific (Waltham, USA). Rotisolv HPLC-gradient grade water, DNA gel loading dye, tris-acetate-EDTA (TAE: 0.4 M tris-acetate, 0.01 M ethylenediaminetetraacetic acid, pH 8.3) buffer and agarose were used from Carl Roth (Karlsruhe, Germany). DNA stain clear G was purchased from Serva (Heidelberg, Germany). MilliQ water was obtained with Milli-Q Reference Water Purification System from Merck Millipore (Burlington, USA). Float-A-Lyzer G2 Dialysis Device (Molecular weight cut-off: 1 kD) was obtained from Spectrum Labs™ (San Francisco, USA).

2.4.2. Irradiation

Irradiation was performed in 0.5 ml tubes with the 17.5 MeV electron beam with increasing doses of up to 60 Gy and a dose rate of 0.05 Gy s^{-1} for conventional dose rate and $2.2 \times 10^5 \text{ Gy s}^{-1}$ for UHDR at 21% O_2 .

2.4.3. Sample preparation and analysis

pBR322 purification was performed with Float-A-Lyzer G2 dialysis device for 24 h at room temperature with HPLC-gradient grade water as a solvent. Afterwards, pBR322 in 20 μl was aliquoted in 0.5 ml tubes (72.704, Sarstedt, Germany).

The 0.8% agarose gel was mixed with 0.004% fluorescent dye Serva DNA stain clear G in $1 \times$ TAE buffer. The solidified agarose gel was loaded with 100 ng pBR322 mixed with 30% loading dye. The gel was submerged in $0.5 \times$ TAE buffer and 100 V voltage applied for 2 h with the EPS 601 (Amersham Pharmacia Biotech, Amersham, Great Britain). The gels were imaged using the Fusion FX7 camera (Vilber, Marne-la-Vallée, France). The DNA content was quantitatively analyzed with image-processing program FusionCapt Advice FX7 (Vilber, Marne-la-Vallée, France). Then the total fluorescent intensities in the three

bands corresponding to the pBR322 conformations—supercoiled (S, no strand break), circular (C, with single-strand break, SSB) and linear (L, with double-strand break, DSB) were quantified. The proportion of each plasmid conformation was thus calculated by integrating the signal over each sample.

2.4.4. Modeling DNA damage

A curve-fitting model by McMahon and Currell (2011) was applied to characterize the SSB and DSB formation in the irradiated plasmid DNA. Briefly, this model operates under the following two assumptions: (1) ionizing events leading to SSB or DSB occur randomly with higher likelihood as dose increases; (2) DSB occurrence is influenced by the probability, denoted as ρ , that multiple SSB arise within a 10-base pair (bp) interval. Given that the formation of SSBs and DSBs is assumed to follow a random distribution, ρ is defined as the ratio of the bp interval (10-base pairs) where two SSBs produce a DSB on the entire pBR322 length (4361-base pairs), giving $\rho = 10/4361$. These assumptions enable the derivation of a set of differential equations, which, upon integration, yield the equations (2)–(4) (McMahon and Currell 2011),

$$S = S_0 e^{-(\beta_S + \beta_D)D}, \quad (2)$$

$$C = e^{-\beta_D D} \left(C_0 e^{-\frac{1}{2}\beta_S^2 \rho D^2} + S_0 \left(e^{-\frac{1}{2}\beta_S^2 \rho D^2} - e^{-\beta_S D} \right) \right), \quad (3)$$

$$L = 1 - (C_0 + S_0) e^{-(\beta_D D + \frac{1}{2}\beta_S^2 \rho D^2)}, \quad (4)$$

where D is the dose, S , C and L are fractional yields of supercoiled, circular and linear conformation of pBR322, respectively, S_0 and C_0 are yields of supercoiled and circular conformation of pBR322 in the control sample, respectively, β_S is the rate of SSBs per Gy, β_D is the rate of DSBs per Gy. Equations (2)–(4) were simultaneously fitted with the evolutionary nonlinear solver in Excel (Microsoft Corporation, Washington, USA) to the experimentally obtained data in order to find values of β_S and β_D , while minimizing error of the fit. Relative biological effectiveness (RBE) of SSB (RBE_{SSB}) was defined as a ratio of the dose delivered by conventional DR (D_{CDR}) to the dose delivered by UHDR (D_{UHDR}) resulting in the same endpoint of 60% SSB, as demonstrated in equation (5),

$$RBE_{SSB} = \frac{D_{CDR}}{D_{UHDR}}. \quad (5)$$

2.5. Design of the full FLASHlab@PITZ beamline

To improve the beam quality, which has been limited on the startup beamline by the dispersion effect from the dipole magnet, a full FLASHlab@PITZ beamline has been designed and is currently undergoing installation. Two objectives have been considered in the design. First, the high quality of the electron beam from the photoinjector must be preserved; and secondly, the beam can be tightly focused at the exit window. As a dipole magnet is already being used to direct the beam to the experimental area on the startup beamline, a natural choice is to add another dipole magnet and quadrupoles in between them to form an achromatic dogleg, which can shift the beam to a parallel beamline while preventing the beam quality from degradation due to dispersion. Two pairs of quadrupole magnets will be installed between the dipoles, with their strengths properly chosen to remove the dispersion (i.e. $\eta_x = 0$, $\eta_{x'} = 0$, where η_x is the dispersion function and $\eta_{x'}$ is the derivative of the dispersion function with respect to the length of path), which is especially critical at higher charges.

Meanwhile, it is also important to monitor and steer the beam, therefore two BPMs, one screen station incorporated with a V-shaped horizontal collimator (which can cut the tails of the beam in the dispersion plane), and two steerer magnets are considered as part of the dogleg, along with pumps for high vacuum and bellows for flexible alignment. To further focus the beam after the dogleg, another two pairs of quadrupoles will be installed and followed by a 2D sweeping system. Several BPMs and two screen stations for beam monitoring, steerers for beam orbit correction, and charge measuring devices such as FCs and ICTs are also being planned there, as shown in the mechanical design in figure 3. It is worth noting that the 2D sweeping system will allow the generation of arbitrary dose distributions with PBS. In addition to that, a specially designed dual-scattering system, which is similar to Robertson *et al* (2023), will allow the generation of uniform dose distributions as well.

To verify the capability of the current design, simulations have been performed at two typical bunch charges. The first is 10 pC, for which the space charge effects are negligible, to be utilized mainly for uniform radiation at conventional dose rates. The other is 1 nC, for which the beam dynamics is dominated by space

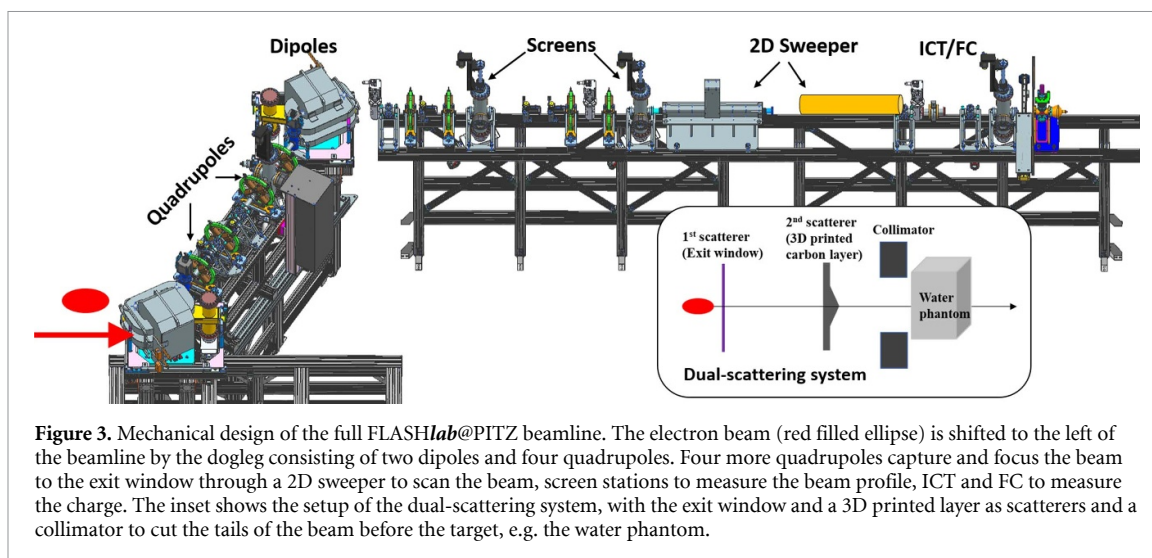


Figure 3. Mechanical design of the full FLASHlab@PITZ beamline. The electron beam (red filled ellipse) is shifted to the left of the beamline by the dogleg consisting of two dipoles and four quadrupoles. Four more quadrupoles capture and focus the beam to the exit window through a 2D sweeper to scan the beam, screen stations to measure the beam profile, ICT and FC to measure the charge. The inset shows the setup of the dual-scattering system, with the exit window and a 3D printed layer as scatterers and a collimator to cut the tails of the beam before the target, e.g. the water phantom.

charge effects, to be utilized mainly for uniform radiation at UHDR. The simulation starts with the optimization of the transverse emittance and the energy spread. Following the emittance compensation concept, the photocathode laser spot size and the focusing magnetic fields from the solenoid coils installed around the RF gun are optimized using the particle tracking code ASTRA (2017). The energy spread can be adjusted by the booster accelerator phase and is nominally minimized at the location of the dogleg. By doing so, the beam size in the dogleg, especially at the first and last quadrupole magnets can be limited. If compression or stretching is required, a slight energy chirp can also be introduced by the booster phase. The beam transport after the booster was performed by the Ocelot code (Agapov *et al* 2014).

One critical condition for the beam transport in the dogleg is the matching of transverse phase space. Due to the limited number of quadrupole magnets in front of the dogleg and their long distance to the first dipole of the dogleg, it is preferred to keep the beam size small with a low divergence at the entrance of the dogleg. On the other side, a relatively large beam size or fast increase of beam size is in favor at the exit of the dogleg, to focus the beam effectively using the following quadrupoles. It is especially critical at high charges in the presence of strong space charge effects. Therefore, the Twiss parameters of the matched beam have been carefully chosen to meet these requirements. The results of start-to-end simulations will be presented in section 3.3. In addition, FLUKA simulations have also been performed using the beam from start-to-end simulations to study the generation of homogeneous dose distributions.

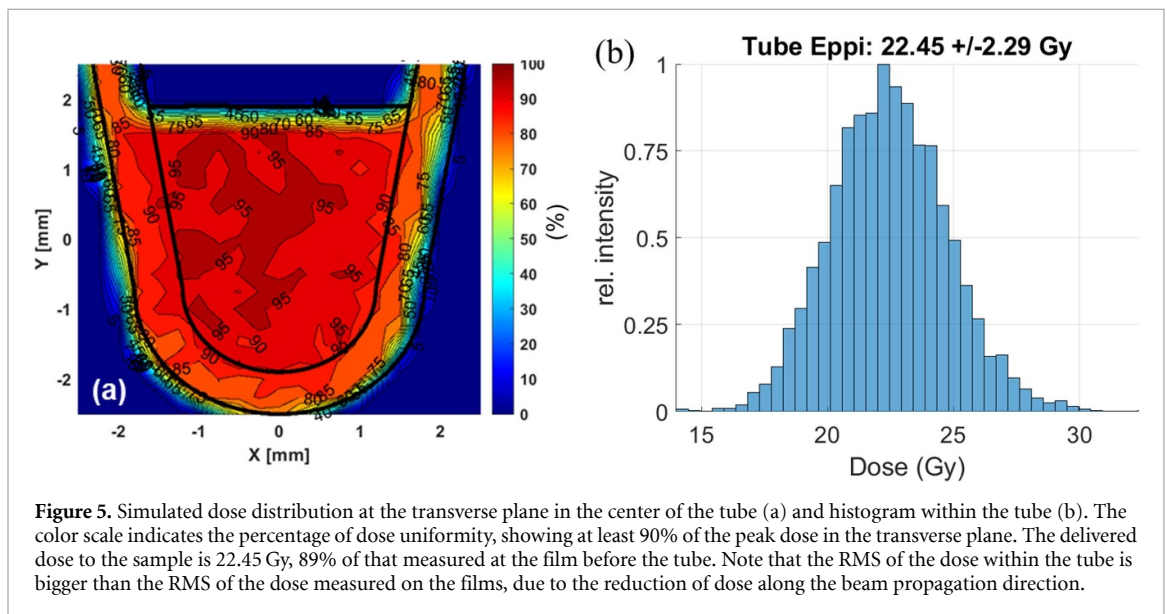
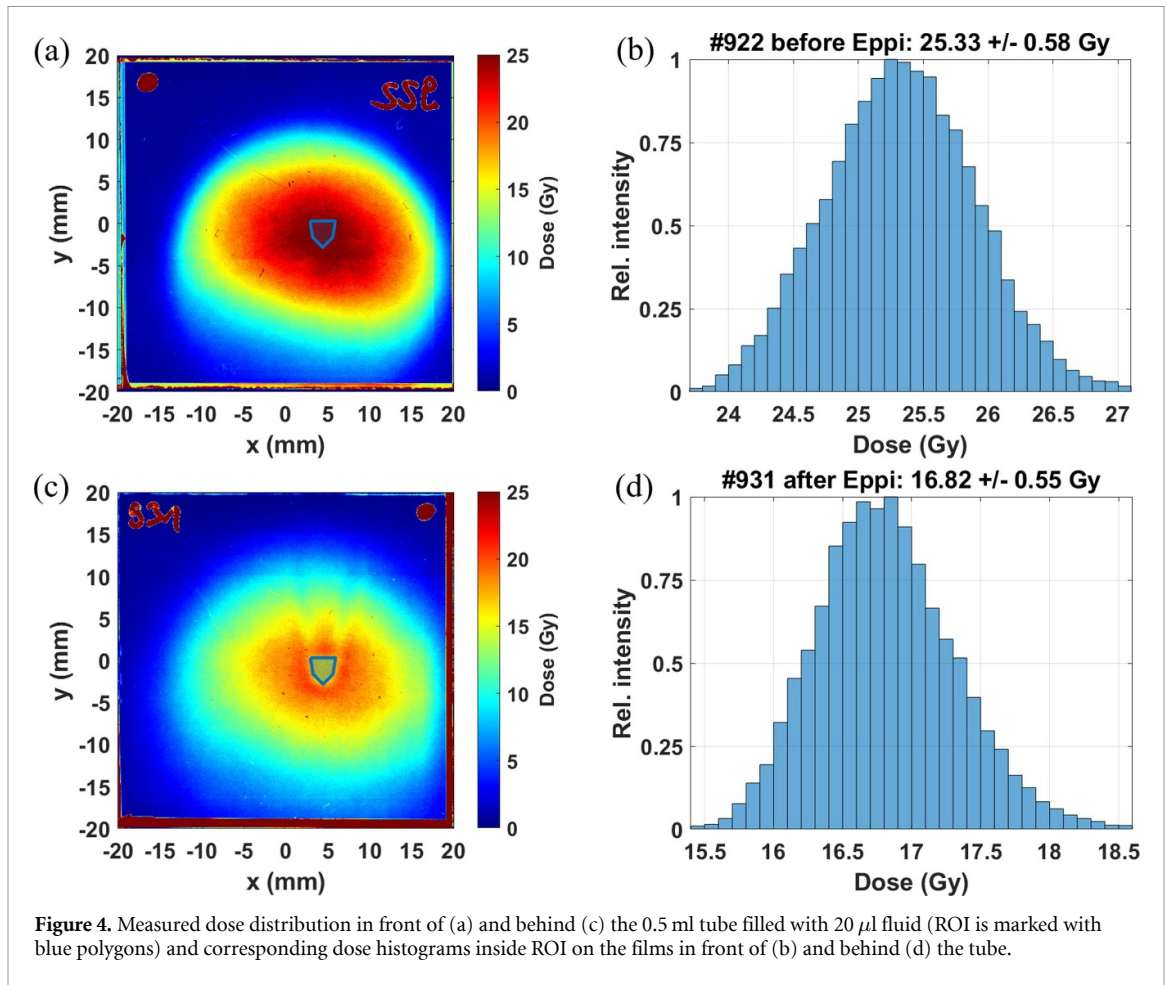
3. Results

3.1. Comparison of dose distributions from measurement and simulations

At FLASHlab@PITZ, films are installed in front of and behind each sample to measure the entrance and exit doses. Upon scanning of the films 24 h after the radiation experiments, the images can be analyzed using self-developed Matlab scripts. Figure 4 shows an evaluated set of films for a high dose rate irradiation ($2.2 \times 10^5 \text{ Gy s}^{-1}$) in plasmid DNA experiments. On the film behind the tube (figure 4(c)), a clear shadow of the tube and the fluid sample inside it is visible. The region of interest (ROI) is then chosen to overlap with the shadow. The exact shape of the ROI is calculated from a 3D model of the tubes and the known sample volume. Since the shadow is only visible on the film behind the tube, it is assumed that the ROI is the same on the film in front of the sample. The dose histograms (figures 4(b) and (d)) show the corresponding dose spectrum only inside the ROI. The delivered dose to the sample was measured as 90% of dose in the ROI on the film in front of the tube, which is regularly checked by putting small film strips directly inside the sample tube.

In addition to dose measurement, FLUKA simulations allow for the estimation of dose uniformity within the sample and the prediction of delivered doses. The simulated results for the same experiment are shown in figure 5, giving a dose distribution with at least 90% of the peak dose in the transverse plane inside the tube. The dose delivered to the sample is 22.45 Gy, considering the tube's shape, 89% of the dose measured from the film in front of the tube (figure 4(b)). This is very close to the measured value of 90%. Therefore this ratio was used in all irradiation experiments.

On the startup beamline, an IC and a diamond detector have also been tested for real-time dose measurement. Additionally, an insertable YAG screen has successfully measured the electron beam



distribution in air. These developments pave the way for real-time determination of dose distribution in the future, integrating both Monte Carlo simulations and experimental measurements.

3.2. Response of plasmid DNA to doses delivered at conventional dose rate and UHDR

Ionizing radiation can directly ionize biomolecules such as DNA and induce reactive oxygen and nitrogen species production (ROS, RNS) that further escalates irreparable intracellular damage and induces the mitotic catastrophe (Buchsbau *et al* 2021, Kacem *et al* 2022, Atkinson *et al* 2023). The isolated plasmid

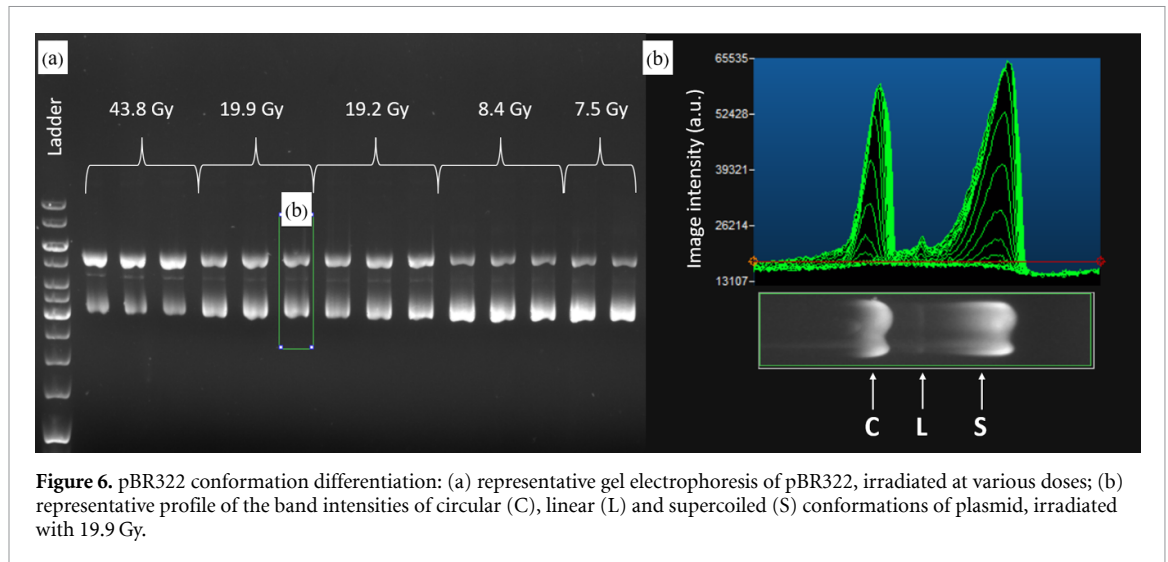


Figure 6. pBR322 conformation differentiation: (a) representative gel electrophoresis of pBR322, irradiated at various doses; (b) representative profile of the band intensities of circular (C), linear (L) and supercoiled (S) conformations of plasmid, irradiated with 19.9 Gy.

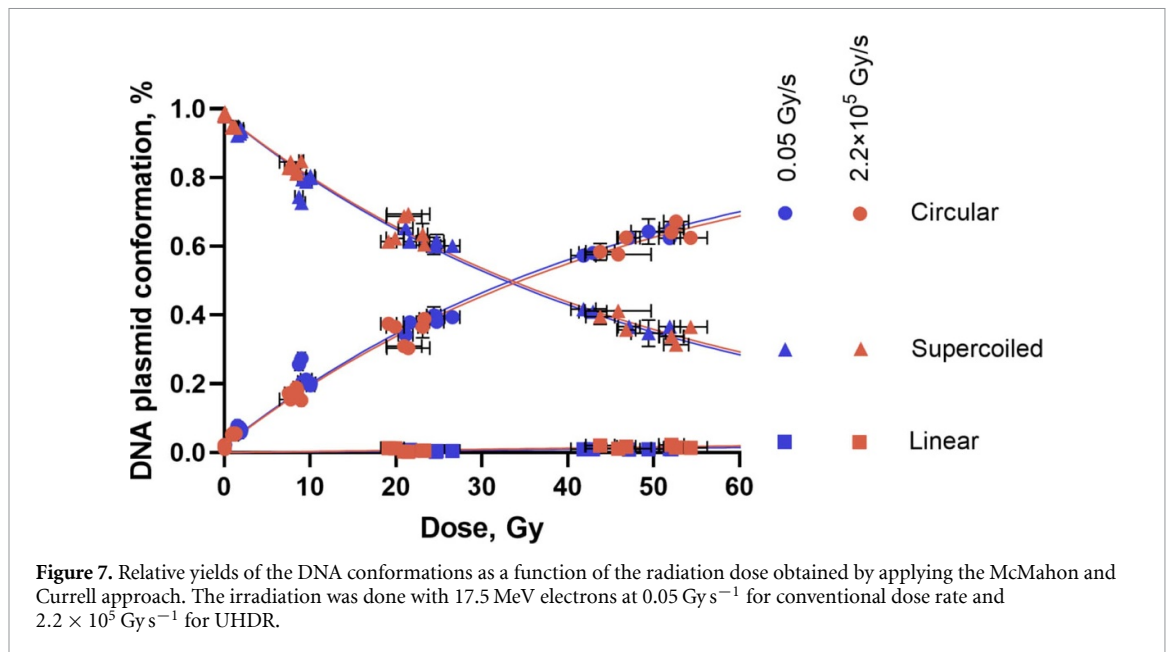


Figure 7. Relative yields of the DNA conformations as a function of the radiation dose obtained by applying the McMahon and Currell approach. The irradiation was done with 17.5 MeV electrons at 0.05 Gy s^{-1} for conventional dose rate and $2.2 \times 10^5 \text{ Gy s}^{-1}$ for UHDR.

found its elegant application as a radiobiological model for assessing DNA damage as its conformations represent the occurrence of single and double-strand breaks (SSB, DSB) in the DNA double helix.

The first investigation on DNA damage of electron UHDR versus conventional electron irradiation at PITZ was performed with 17.5 MeV electrons at the startup beamline, with plasmid DNA, pBR322 at 0.05 Gy s^{-1} and $2.2 \times 10^5 \text{ Gy s}^{-1}$ with a dose up to 60 Gy. The conformations of plasmid DNA in the samples were separated with gel electrophoresis and analyzed, as shown in figure 6.

Figure 7 demonstrates the yields of supercoiled, circular and linear conformations of irradiated pBR322 by applying the McMahon and Currell DNA damage fitting model (McMahon and Currell 2011). The circular conformation (with one SSB) accounted $1.39 \pm 0.51\%$ of non-irradiated plasmid that evidenced its high quality. The observed conformation yields of the irradiated plasmid DNA revealed its dose-dependent radiation damage. The relative amount of circular conformation was increased with higher doses with respective drop in supercoiled conformation yield (no strand breaks). The linear conformation (with DSB) was detectable from 20 Gy. Similar DNA damage patterns were found for both explored conventional and UHDR radiation. The McMahon and Currell curve-fitting model applied to the obtained data yielded the β and RBE parameters for SSB given in table 3, confirming the similar effects of conventional and UHDR electron irradiation.

However, the difference between the assessed DSB yields under conventional and UHDR radiation is not significant, pointing to the need of further dose-escalation studies and plasmid preparation optimization.

Table 3. SSB induction rate in pBR322 by conventional and UHDR electron irradiation.

Irradiation mode	Dose rate, Gy s ⁻¹	$\beta_S, \times 10^{-2}$ Gy ⁻¹ ^a	RBE _{SSB} ^a
CONV	0.05	1.99 ± 0.04	1
UHDR	2.2 × 10 ⁵	2.04 ± 0.07	1.04 ± 0.06

^a Computed with the McMahon and Currell curve-fitting model.

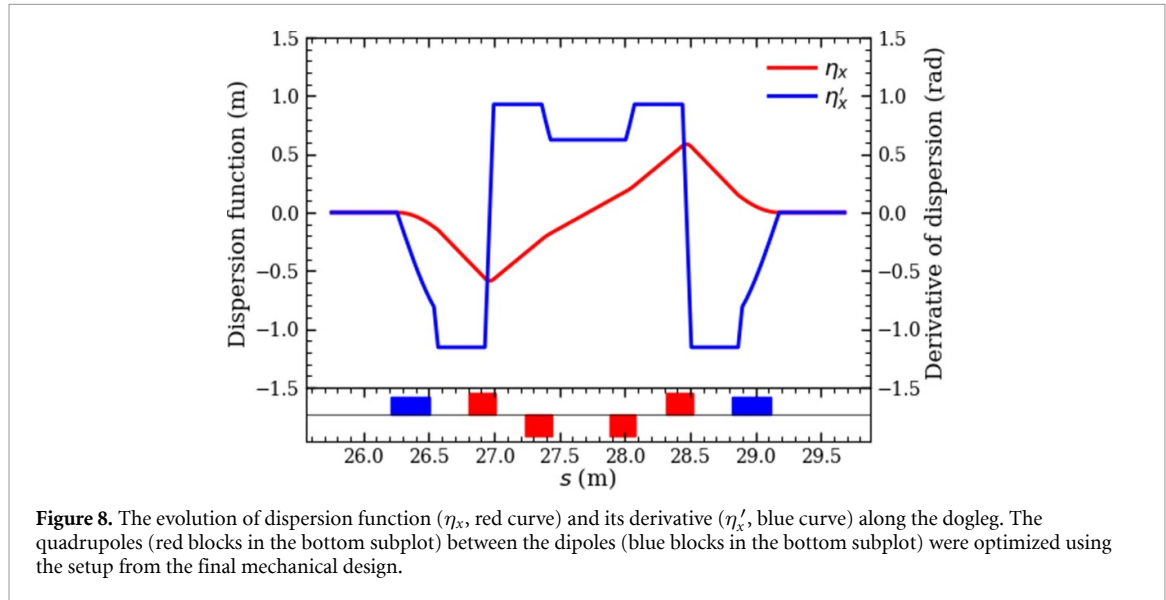


Figure 8. The evolution of dispersion function (η_x , red curve) and its derivative (η'_x , blue curve) along the dogleg. The quadrupoles (red blocks in the bottom subplot) between the dipoles (blue blocks in the bottom subplot) were optimized using the setup from the final mechanical design.

3.3. Simulated performance of the full FLASHlab@PITZ beamline

For the full beamline, preliminary simulations have been done for a huge charge range (from pC to 5 nC) using the beam optics from our initial physics design, as discussed in Li *et al* (2022). The beam optics have been modified a lot during the mechanical design to give space for beam manipulation/diagnostics devices and vacuum parts. Following the mechanical design, the quadrupoles in the dogleg have been optimized, and the resulting dispersion curves are shown in figure 8. Note that the transfer matrix of the achromatic dogleg has a nonzero R_{56} (0.105 m in this case), which will allow for tuning the bunch length by introducing an energy chirp in the longitudinal phase space.

For both 10 pC and 1 nC, the beam emittance has been minimized in the photoinjector. The beam transport after the booster accelerator and beam matching into the dogleg has been optimized to minimize the beam emittance growth from space charge effects over the beamline and dispersion effect in the dogleg. The results are shown in figure 9, where the RMS beam sizes of the beam from the photocathode to the exit window are shown and the beam distributions at the exit window are given. For 10 pC, an RMS beam size as small as 50 μm is possible; for 1 nC, the minimal RMS beam size is 0.3 mm. The two distributions are further used for Monte Carlo simulations to demonstrate the promising dose distributions in different irradiation scenarios.

As mentioned earlier, the FLASHlab@PITZ beamline will enable the generation of dose distributions in two substantially different manners within one RF pulse of less than 1 ms. Both have been studied by Monte Carlo simulations using FLUKA. The simulation setups and relevant electron beam and dose parameters are summarized (Böhlen *et al* 2024) in table 4.

The percentage dose depth curves from FLUKA simulations are shown in figure 10. In both cases, more than 90% of the maximum dose is reached within 2 cm depth and around 80% of the dose reached within 4 cm depth into the water phantom. The peak from scanning beams comes later because the electrons are less diverging when entering the water. The 2D dose distributions from FLUKA simulations are shown in figure 11 and a sharp reduction of dose is observed at the border of the areas of interest, which will minimize the radiation effects on the surrounding experimental setup or the normal tissues in cancer studies. It is worth noting that the area of uniform distribution can be easily scaled up and down. Compared to dose distributions shown in figure 4, the distribution can be confined within the tip of tubes. In addition, in the simulations, only limited numbers of electron bunches and limited bunch charges were considered. By employing the maximum number and charge of electron bunches, the dose at the reference point can reach more than 1000 Gy within 1 ms from both scanning beams and scattering beams. By adjusting the repetition

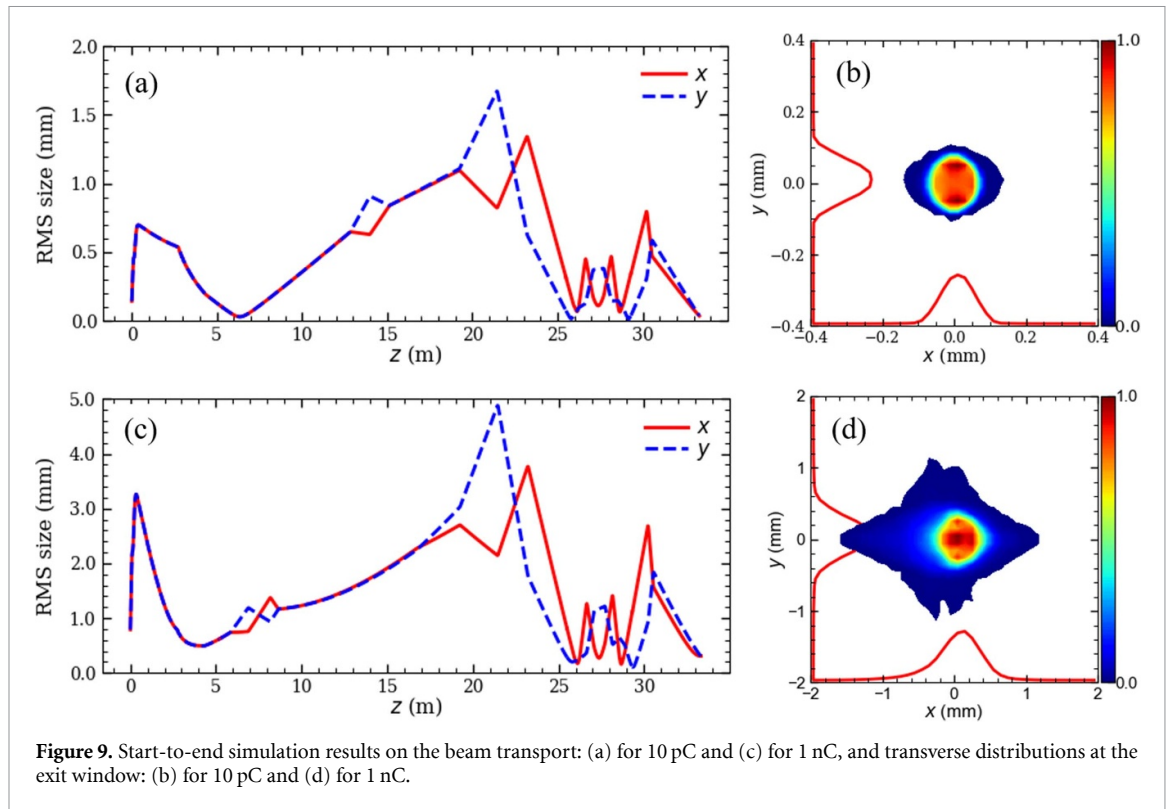


Figure 9. Start-to-end simulation results on the beam transport: (a) for 10 pC and (c) for 1 nC, and transverse distributions at the exit window: (b) for 10 pC and (d) for 1 nC.

Table 4. Summary of the electron beams and simulated doses.

Parameter	Scanning beams	Scattering & Collimation ^a
Bunch charge	40 pC	1 nC
Bunch energy	17.5 MeV	17.5 MeV
Bunch repetition rate	4.5 MHz	4.5 MHz
Number of bunches	25 × 25	38
Radiation time	138.7 μ s	8.2 μ s
Dose at reference point	10 Gy	10 Gy
Reference point	1 cm depth in water phantom, which is 3 cm downstream of the exit window	1 cm depth in the water phantom located 35 cm downstream of the exit window
Field size	Squared, 2 cm × 2 cm (>90% of the maximum dose)	Circular with a diameter of 2 cm (>90% of maximum dose)
Average dose rate at reference point	0.518×10^6 Gy s ⁻¹ ^b	1.21×10^6 Gy s ⁻¹

^a A dual-scattering system (figure 3) was optimized with a special scatterer inserted at 20 cm downstream of the exit window and a collimator with a diameter of 2.2 cm and thickness of 5 cm right before the water surface.

^b The dose rate is calculated following the method in Folkerts *et al* (2020).

rate of the bunches with the bunch pattern server, as illustrated in figure 1, the dose rate can also be scaled down easily.

4. Discussion

Dosimetry studies using Gafchromic films and FLUKA simulations and biochemical experiments with plasmid DNA have been performed on the startup beamline at FLASHlab@PITZ. A transverse uniform dose distribution (>90%) has been delivered to the samples at conventional dose rate (0.05 Gy s⁻¹) and UHDR (2.2×10^5 Gy s⁻¹) with a maximum dose up to 60 Gy.

Currently, the dose in the sample is estimated from measured dose inside a selected area on the film in front of the tube. The area is determined by the shadow in the dose distribution measured by the film after the tube. The misalignment of the two films due to the errors in cutting and installing the films and subsequently the selected area on the front film introduced an error to the dose estimation, which partially

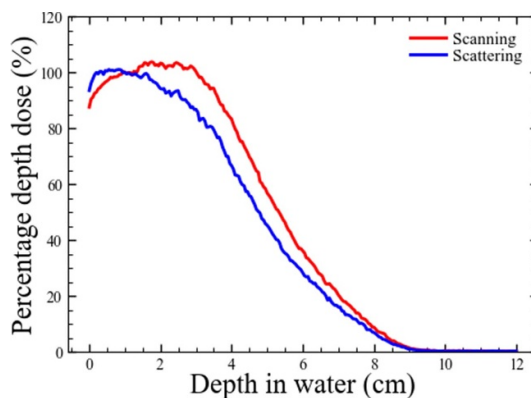


Figure 10. Percentage depth dose normalized to the reference point (volume resolution 1 mm^3) along the central beam axis for scanning beams (red curve) and scattered beams (blue curves).

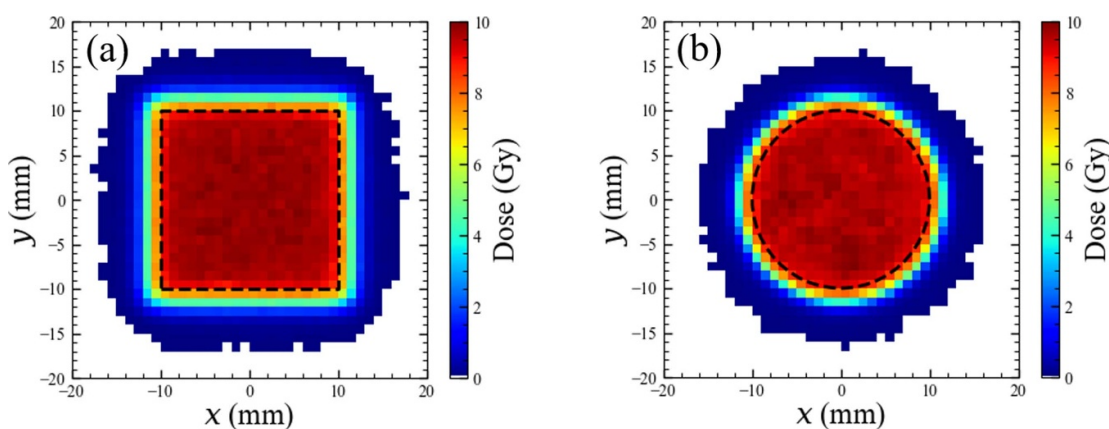


Figure 11. 2D dose distributions (volume resolution 1 mm^3) at the depth of 1 cm inside water generated by (a) scanning and (b) scattered beams. The dashed black lines illustrated the area of $2 \text{ cm} \times 2 \text{ cm}$ in (a) and a circle of 2 mm diameter in (b) with more than 90% of the maximum dose.

led to the disagreement between the measured and simulated doses. This will be improved with a new tube holder, with a special design to locate the corresponding area of doses on the front film directly. In addition, the 24 h waiting time before scanning the Gafchromic films makes it impossible to measure the dose online. By using the IC, which is calibrated with the measurements by the films, online dose determination will be possible soon.

The biochemical experiments, which evaluated the strand breaks in the plasmid DNA (pBR322) induced by radiations, have delivered a proof-of-concept for biomedical research at the startup beamline. Up to 60 Gy doses were delivered to pBR322 in 20 ml at 21% O_2 and induced dose-dependent DNA damage. The observed SSB and DSB yields were increasing with higher doses similarly for both conventional dose rate and UHDR. Comparably, in pure water and under atmospheric and physoxic condition, 6 MeV electron irradiation caused similar plasmid DNA damage for both 0.01 Gy s^{-1} in conventional dose rate and $5.6 \times 10^6 \text{ Gy s}^{-1}$ in UHDR (Cherbuin *et al* 2021). Small *et al* observed no significant variations in 1 mM Tris between DSB yields in plasmid irradiated by electron beams of three energies (100, 150 and 200 MeV) at the conventional dose rate of 0.5 Gy s^{-1} and UHDR of $>10^8 \text{ Gy s}^{-1}$ but reduced SSB yields at the beam energy of 100 MeV at the conventional dose rate (2021). The study by Perstin *et al* evidenced the DNA damage-sparing ability of 16 MeV electron irradiation with 46.6 and 93.2 Gy s^{-1} as compared with the conventional dose rate of 0.167 Gy s^{-1} in plasmid in 0.48 mM Tris (2022). In another study by Ohsawa *et al*, plasmid DNA in 10 mM Tris, 1 mM EDTA and irradiated with 27.5 MeV proton beam at 40 Gy s^{-1} had reduced SSB but not DSB as compared to conventional dose rate of 0.05 Gy s^{-1} (2021). Kacem *et al* reported the reduced plasmid damage in 14 mM Dimethylsulfoxide, that was dose-rate independent for radiations with electron beams of 5.5 MeV (0.1 versus $\geq 555 \text{ Gy s}^{-1}$) and 200 MeV (0.2 versus $4.55 \times 10^8 \text{ Gy s}^{-1}$) (2024).

The varying data of UHDR ability to spare DNA from radiation damage highlights the challenge to mimic *in vivo* conditions with simplified *in vitro* models. The growing body of evidence points that the radiolytic damage of DNA molecules is to be performed in strictly controlled chemical buffer composition to mimic

redox-oxidant status of intracellular or extracellular environment that also varies among normal and cancer tissues. The observed delayed DNA damage along the delivered doses in the presented data as compared to previous studies pointed to the possible significant remaining content of the plasmid storage buffer even after dialysis that scavenged generated ROS during irradiation. Hence, further investigation into the effect of the buffer composition and oxygen level as well as electron beam parameter space, including but not limited to delivered dose, pulse duration and frequency, mean and instantaneous dose rate are of high interest.

The upgrade of the startup beamline to the full FLASHlab@PITZ beamline and subsequently better electron beam properties will provide the capability of exploring such parameter ranges. The designed performance of the new beamline has been confirmed by start-to-end simulations, with wide and uniform dose distributions generated by both scanning beams and scattering beams.

5. Conclusion

The photoinjector test facility at DESY in Zeuthen can provide electron beams with a hugely adjustable bunch charge and flexible bunch time structure, which allows to generate a uniquely wide dose parameter space for systematically studying the FLASH effect in cancer treatment. Some basic capabilities of electron beam delivery, dose prediction and measurement for radiation experiments have been demonstrated on the startup beamline, where radiation effects on plasmid DNA have been studied under various doses up to 60 Gy at the conventional dose rate of 0.05 Gy s^{-1} and UHDR of $2.2 \times 10^5 \text{ Gy s}^{-1}$ within one RF pulse of up to 1 ms length. An upgrade of the startup beamline to a full beamline is undergoing construction. The performance of the new beamline has been verified by start-to-end simulations, promising a more flexible dose generation by PBS or by scattering and collimating.

Data availability statement

All data that support the findings of this study are included within the article (and any supplementary information files).

ORCID iDs

X-K Li  <https://orcid.org/0000-0002-5487-688X>
Y Komar  <https://orcid.org/0009-0007-8251-4222>
P Borchert  <https://orcid.org/0009-0009-8156-3131>
D Dmytriiev  <https://orcid.org/0000-0003-3612-2686>
G Loisch  <https://orcid.org/0000-0002-6178-2339>
Z Lotfi  <https://orcid.org/0000-0002-6217-9742>

References

- Agapov I, Geloni G, Tomin S and Zagorodnov I 2014 OCELOT: a software framework for synchrotron light source and FEL studies *Nucl. Instrum. Methods Phys. Res. A* **768** 151–6
- Atkinson J, Bezak E, Le H and Kempson I 2023 The current status of FLASH particle therapy: a systematic review *Phys. Eng. Sci. Med.* **46** 529–60
- Beckmann I A 2020 Die blauen ratgeber: Strahlentherapie (available at: www.krebshilfe.de)
- Beyreuther E, Brand M, Hans S, Hideghéty K, Karsch L, Lefmann E, Schürer M, Szabó E and Pawelke J 2019 Feasibility of proton FLASH effect tested by zebrafish embryo irradiation *Radiother. Oncol.* **139** 46–50
- Bley C R et al 2022 Dose- and volume-limiting late toxicity of FLASH radiotherapy in cats with squamous cell carcinoma of the nasal planum and in mini pigs *Clin. Cancer Res.* **28** 3814–23
- Böhlen T T et al 2024 Recording and reporting of ultra-high dose rate “FLASH” delivery for preclinical and clinical settings *Radiother. Oncol.* **200** 110507
- Bourhis J et al 2019 Treatment of a first patient with FLASH-radiotherapy *Radiother. Oncol.* **139** 18–22
- Bray F, Laversanne M, Sung H, Ferlay J, Siegel R L, Soerjomataram I and Jemal A 2024 Global cancer statistics 2022: GLOBOCAN estimates of incidence and mortality worldwide for 36 cancers in 185 countries *CA Cancer J. Clin.* **74** 229–63
- Buchsbaum J, Coleman C, Espey M, Prasanna P, Capala J, Ahmed M, Hong J and Obcemea C 2021 FLASH radiation therapy: new technology plus biology required *Int. J. Radiat. Oncol.* **110** 1248–9
- Cherbuin N, Ollivier J, Jorge P, Grilj V, Chappuis F, Desorgher L, Bailat C, Bochud F, Pires J and Vozenin M 2021 Plasmid DNA damages after FLASH vs conventional dose rate irradiations in various oxygen conditions *ESTRO*
- Cunningham S et al 2021 FLASH proton pencil beam scanning irradiation minimizes radiation-induced leg contracture and skin toxicity in mice *Cancers* **13** 1012
- Darafsheh A, Hao Y, Zhao X, Zwart T, Wagner M, Evans T, Reynoso F and Zhao T 2021 Spread-out Bragg peak proton FLASH irradiation using a clinical synchrocyclotron: proof of concept and ion chamber characterization *Med. Phys.* **48** 4472–84
- Daugherty E C et al 2023 FLASH radiotherapy for the treatment of symptomatic bone metastases (FAST-01): protocol for the first prospective feasibility study *JMIR Res. Protoc.* **12** e41812
- Daugherty E C et al 2024 FLASH radiotherapy for the treatment of symptomatic bone metastases in the thorax (FAST-02): protocol for a prospective study of a novel radiotherapy approach *Radiat. Oncol.* **19** 34

- Diffenderfer E S *et al* 2020 Design, Implementation and *in vivo* validation of a novel proton FLASH radiation therapy system *Int. J. Radiat. Oncol. Biol. Phys.* **106** 440–8
- Fasso A, Ferrari A, Ranft J and Sala R P 2005 (CERN) FLUKA: a multi-particle transport code (program version 2005) *Technical Report CERN-2005-10*
- Favaudon V *et al* 2014 Ultrahigh dose-rate FLASH irradiation increases the differential response between normal and tumor tissue in mice *Sci. Transl. Med.* **6** 245ra93
- Floettmann K 2017 Astra: a space charge tracking algorithm version 3.2 (available at: www.desy.de/~mpyflo/)
- Folkerts M, Abel E, Busold S, Perez J, Krishnamurthi V and Ling C 2020 A framework for defining FLASH dose rate for pencil beam scanning *Med. Phys.* **47** 6396–404
- GAFCHROMIC™ DOSIMETRY MEDIA, TYPE EBT-XD, *Specification and User Guide* (available at: gafchromic.com)
- Gao F *et al* 2022 First demonstration of the FLASH effect with ultrahigh dose rate high-energy x-rays *Radiother. Oncol.* **166** 44–50
- Kacem H *et al* 2024 Modification of the microstructure of the CERN-CLEAR-VHEE beam at the picosecond scale modifies ZFE morphogenesis but has no impact on hydrogen peroxide production *bioRxiv Preprint* <https://doi.org/10.1101/2024.12.19.629203> (posted online 20 December 2024)
- Kacem H, Almeida A, Cherbuin N and Vozenin M-C 2022 Understanding the FLASH effect to unravel the potential of ultra-high dose rate irradiation *Int. J. Radiat. Biol.* **98** 506–16
- Kilmister E, Koh S, Weth F, Gray C and Tan S 2022 Cancer metastasis and treatment resistance: mechanistic insights and therapeutic targeting of cancer stem cells and the tumor microenvironment *Biomedicines* **10** 2988
- Konradsson E, Liljedahl E, Gustafsson E, Adrian G, Beyer S, Ilaahi S, Petersson K, Ceberg C and Redebrandt H N 2022 Comparable long-term tumor control for hypofractionated FLASH versus conventional radiation therapy in an immunocompetent rat glioma model *Adv. Radiat. Oncol.* **7** 101011
- Korysko P, Bateman J, Robertson C and Dosanjh M 2023 VHEE and ultra high dose rate radiotherapy studies in the clear user facility *Proc. IPAC'23* pp 5063–6
- Lempart M, Blad B, Adrian G, Bäck S, Knöös T, Ceberg C and Petersson K 2019 Modifying a clinical linear accelerator for delivery of ultra-high dose rate irradiation *Radiother. Oncol.* **139** 40–45
- Li X K *et al* 2022 Physics design of electron FLASH radiation therapy beamline at PITZ *Proc. IPAC'22* vol 13 pp 2954–7
- Li X K *et al* 2024 Overview of FLASHlab@PITZ: the new R&D platform for FLASH radiation therapy and radiation biology *J. Phys.: Conf. Ser.* **2687** 092006
- McMahon S and Currell F 2011 A robust curve-fitting procedure for the analysis of plasmid DNA strand break data from gel electrophoresis *Radiat. Res.* **175** 797–805
- Metzkes-Ng J *et al* 2023 The DRESDEN PLATFORM is a research hub for ultra-high dose rate radiobiology *Sci. Rep.* **13** 20611
- Moeckli R, Gonçalves Jorge P, Grilj V, Oesterle R, Cherbuin N, Bourhis J, Vozenin M-C, Germond J-F, Bochud F and Bailat C 2021 Commissioning of an ultra-high dose rate pulsed electron beam medical LINAC for FLASH RT preclinical animal experiments and future clinical human protocols *Med. Phys.* **48** 3134–42
- Montay-Gruel P *et al* 2017 Irradiation in a flash: unique sparing of memory in mice after whole brain irradiation with dose rates above 100 Gy/s *Radiother. Oncol.* **124** 365–9
- Montay-Gruel P *et al* 2018 x-rays can trigger the FLASH effect: ultra-high dose-rate synchrotron light source prevents normal brain injury after whole brain irradiation in mice *Radiother. Oncol.* **129** 582–8
- Ohsawa D, Hiroshima Y, Kobayashi A, Kusumoto T, Kitamura H, Hojo S, Kodaira S and Konishi T 2021 DNA strand break induction of aqueous plasmid DNA exposed to 30 MeV protons at ultra-high dose rate *J. Radiat. Res.* **63** 255–60
- Patriarca A *et al* 2018 Experimental set-up for FLASH proton irradiation of small animals using a clinical system *Int. J. Radiat. Oncol. Biol. Phys.* **102** 619–26
- Perstin A, Poirier Y, Sawant A and Tambasco M 2022 Quantifying the DNA-damaging effects of FLASH irradiation with plasmid DNA *Int. J. Radiat. Oncol.* **113** 437–47
- Robertson C *et al* 2023 Dual-scattering foil installation at CLEAR *Proc. IPAC'23* vol 14 pp 5059–62
- Schüler E, Trovati S, King G, Lartey F, Rafat M, Villegas M, Praxel A, Loo B and Maxim P 2017 Experimental platform for ultra-high dose rate FLASH irradiation of small animals using a clinical linear accelerator *Int. J. Radiat. Oncol. Biol. Phys.* **97** 195–203
- Schulz A, Meyer F, Dubrovskaya A and Borgmann K 2019 Cancer stem cells and radioresistance: DNA repair and beyond *Cancers* **11** 862
- Small K L *et al* 2021 Evaluating very high energy electron RBE from nanodosimetric pBR322 plasmid DNA damage *Sci. Rep.* **11** 3341
- Stephan F *et al* 2022 FLASHlab@PITZ: new R&D platform with unique capabilities for electron FLASH and VHEE radiation therapy and radiation biology under preparation at PITZ *Phys. Medica* **104** 174–87
- Vozenin M-C *et al* 2019 The advantage of FLASH radiotherapy confirmed in mini-pig and cat-cancer patients *Clin. Cancer Res.* **25** 35–42
- Zhang Q, Cascio E, Li C, Yang Q, Gerweck L, Huang P, Gottschalk B, Flanz J and Schuemann J 2020 FLASH investigations using protons: design of delivery system, preclinical setup and confirmation of FLASH effect with protons in animal systems *Radiat. Res.* **194** 656–64